Conformation of Myosin Interdomain Interactions during Contraction: Deductions from Proteins in Solution†

Thomas P. Burghardt,* Sungjo Park, and Katalin Ajtai

Department of Biochemistry and Molecular Biology, Mayo Foundation, 200 First Street SW, Rochester, Minnesota 55905

Received October 16, 2000; Revised Manuscript Received January 4, 2001

ABSTRACT: Myosin subfragment 1 (S1) is the ATP catalyzing motor protein in muscle. It consists of three domains that catalyze ATP and bind actin (catalytic), conduct energy transduction (converter), and transport the load (lever arm). These domains interface in two places identified as interface I, containing the reactive thiol (SH1) and ATP-sensitive tryptophan (Trp510), and interface II, containing the reactive lysine residue (RLR). Two crystal structures of S1 were extrapolated to working "in solution" or oriented "in tissue" forms, using structure-sensitive optical spectroscopic signals from extrinsic probes located in the interfaces. Observed signals included circular dichroism (CD) and absorption originating from S1 in solution in the presence and absence of actin and fluorescence polarization from cross-bridges in muscle fibers. Theoretical signals were calculated from S1 crystal structure models perturbed with lever arm movement from swiveling at three conserved glycines, 699, 703, and 710 (chicken skeletal myosin numbering). Structures giving the best agreement between the computed and observed signals were selected as the representative forms. Both interfaces undergo dramatic conformational change during ATPase and force development. Changes at interface I suggest the molecular basis for the collisional quenching sensitivity of Trp510 to nucleotide binding. The probe conformation at SH1 suggests how it alters S1 ATPases. At interface II, the spatial relationship of the lever arm and the extrinsic probe at RLR suggests how the probe alters S1 ATPases and that it should inhibit lever arm movement during the power stroke. The latter possibility, if true, establishes a part of the corridor through which the lever arm swings during the power stroke. Global structural changes in actomyosin are discussed in the accompanying paper [Burghardt et al. (2001) *Biochemistry 40,* 4821−4833].

Skeletal myosin is a motor protein functioning in muscle as the chemomechanical energy transducer (*2*). As such, this protein, in association with actin, transduces the chemical energy in ATP to mechanical work. The globular head of the myosin cross-bridge, when cleaved from its tail portion to produce myosin subfragment 1 (S1),[1] competently carries out all of its functions (*3*). For this reason, S1 is thought to contain all of the necessary elements of the motor except possibly for those residing in the actin (*4*). Crystal structures of S1 suggest that it is made up of three regions that catalyze ATP and bind actin (catalytic), conduct energy transduction (converter), and transport the load (lever arm) (*5*−*7*). Catalytic, converter, and lever arm domains interface in two places identified as interfaces I and II in Figure 1. Interface I is the probe binding cleft containing the reactive thiol (SH1 or Cys707) and the ATP-sensitive tryptophan (Trp510) (*8*−*14*). Interface II contains the reactive lysine residue (RLR or Lys84) (*15*−*22*). We wish to correlate the structure of these interfaces with steps in the contraction cycle, including

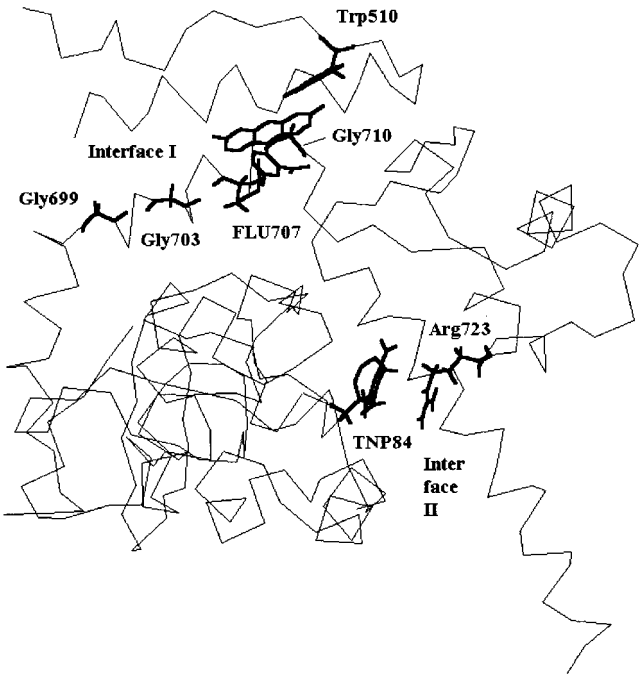

FIGURE 1: α-Carbons and selected side chains (bolded) of modified skeletal S1. Interface I contains the ATP-sensitive tryptophan (Trp510), IAF modifying the reactive thiol (FLU707), and glycine swivels at 699, 703, and 710. Interface II contains the reactive lysine residue modified with TNP (TNP84) and Arg723.

† This work was supported by National Institutes of Health Grant R01 AR39288 and the Mayo Foundation.

* Corresponding author: phone 507 284 8120; fax 507 284 9349; e-mail burghardt@mayo.edu.

[1] Abbreviations: AlF_4^-, aluminum fluoride complex; BeF_x, beryllium fluoride complex; CD, circular dichroism; DcS1, dictyostelium myosin subfragment 1; F-S1, 5′-iodoacetamidofluorescein-labeled most reactive thiol in myosin subfragment 1; IAF, 5′-iodoacetamidofluorescein; RLR, reactive lysine residue (Lys84); S1, myosin subfragment 1; SH1, most reactive thiol in myosin subfragment 1 (Cys707); TNBS, 2,4,6-trinitrobenzenesulfonic acid; TNP-S1, TNBS-labeled reactive lysine residue in myosin subfragment 1; Trp510, ATP-sensitive tryptophan in chicken pectoralis muscle. Myosin sequence numbering throughout the paper is that of chicken pectoralis muscle (*1*).

10.1021/bi002388g CCC: $20.00
Published on Web 03/22/2001

force generation, to obtain a dynamical picture of the molecular mechanism of chemomechanical energy transduction over a cross-bridge cycle. To carry out this objective, we structurally characterize signals from extrinsic spectroscopic probes located in each interface.

Structural characterization of interfaces I and II is one part of a larger task we have undertaken to investigate the energy transduction mechanism. We have found it convenient to separate aspects of myosin energy transduction into two categories: one related to local conformation changes, the subject of this paper, and a second related to global conformational change in myosin, the subject of the accompanying paper referred to subsequently as part 1 (*23*). The work described here and in part 1 demonstrates how extrinsic spectroscopic probes of myosin offer a look into structural changes accompanying energy transduction that elucidate both local and global features of the process. The choice of system from which myosin is observed and the spectroscopic signal detected determine the relevance of the data to local or global S1 conformation.

Circular dichroism (CD) is a structurally interpretable signal originating in our system from the Cotton effect induced in the absorption band of the probe (*24*). S1 alone or in association with F-actin in solution is a convenient system for use with CD because its macroscopic disorder minimizes artifactual optical activity due to birefringence. We have used CD from two probes (one of which is also the global cross-bridge positioning probe used in part 1) reporting from interfaces I and II in the past and have already observed that these interfacial regions change conformation dramatically during ATP hydrolysis (*15*, *25*). Now we introduce actin to the system to mimic contracting muscle fiber conditions.

Although we have presented our findings on the global features of energy transduction in part 1, the actoS1 structures shown and discussed there are partially the consequence of data we present in this paper. Likewise, data from the accompanying paper influence the probe/protein structures shown and discussed here. This is so because they are the same S1 conformations satisfying the structural constraints provided by the integrated spectroscopic signals from the probes of S1 when the protein is free in solution and when it is part of a muscle fiber cross-bridge. The combined data provide more structural constraints enabling us to surmise a more reliable model for the conformation changes in S1 accompanying energy transduction. How we formulated the signal integration is discussed in part 1.

MATERIALS AND METHODS

Chemicals. ATP, ADP, sodium azide, $BeCl_2$ (dissolved in 1% HCl), α-chymotrypsin, dimethyl sulfoxide (DMSO), dithiothreitol (DTT), HEPES, phenylmethanesulfonyl fluoride (PMSF), and Tris are from Sigma (St. Louis, MO). 2,4,6-Trinitrobenzenesulfonic acid (TNBS) is from Fluka (Milwaukee, WI). 5′-Iodoacetamidofluorescein (IAF) is from Molecular Probes (Eugene, OR). ATPγS is from Roch Molecular Biochemicals (Indianapolis, IN). The ADP contamination of the ATPγS is less than 5% according to polyethylenimine−cellulose thin-layer chromatography (PEI TLC). All other chemicals are of reagent grade. Potassium fluoride (KF) stock solution was prepared on the day it was used. PD10 Sephadex G-25 columns are from Amersham Pharmacia Biotech (Uppsala, Sweden).

Preparation of Proteins. Rabbit myosin was prepared from back and leg muscles by the methods of Tonomura et al. (*26*). S1 was obtained by digestion of myosin filaments with α-chymotrypsin as described by Weeds and Taylor (*27*). G-actin was prepared by a standard protocol from rabbit skeletal muscle acetone powder (*28*). The S1 used in our experiments contains a mixture of isoenzymes. Protein concentrations were obtained with absorbance using an $A(1\%)$ at 280 nm of 5.5 and 7.45 for myosin and S1, respectively, and $A(1\%)$ at 290 nm of 6.4 for actin. Molecular masses were assumed to be 450, 115, and 42 kDa for myosin, S1, and actin.

ATPase Assay. ATPase activity of S1 was measured from organic phosphate production using the Fiske and Subbarow method and expressed as percent of control S1 (*29*). K^+-EDTA ATPase measurements were made on samples at 25 °C from 1 mL aliquots containing 0.26−0.35 μM S1, 2 mM ATP, 0.6 M KCl, 6 mM EDTA, and 25 mM Tris-HCl at pH 8. Ca^{2+}-ATPase was measured as for K^+-EDTA ATPase except 6 mM $CaCl_2$ replaced EDTA. When estimating the inhibition of the ATPase due to active site trapping, Ca^{2+}-ATPase was measured with 20 mM $CaCl_2$ to avoid competition from Mg. Mg^{2+}-ATPase measurements were made on samples at 25 °C from 1 mL aliquots containing 4−13 μM S1, 4 mM ATP, 0.1 M KCl, 4 mM $MgCl_2$, and 25 mM Tris-HCl at pH 8 and without a deproteinization step as suggested by Tashima (*30*).

Chemical Modification of Proteins. S1 was trinitrophenylated according to published protocols (*20*, *21*). A 2-fold molar excess of TNBS was added to 60−80 μM S1 in 30 mM KCl, 0.2 mM PMSF, and 100 mM Tris-HCl buffer, pH 7.8. After incubation at 25 °C for 10 min the reaction was terminated by addition of 2 mM DTT. Excess TNBS was removed by dialyzing twice against 100 volumes of 1 mM DTT, 60 mM KCl, 0.1 mM PMSF, and 30 mM HEPES buffer, pH 7.0 at 4 °C (without DTT in the second dialysis). The number of TNP groups introduced was obtained from absorbance at 345 nm using $\epsilon_{345} = 14\,500\ M^{-1}\ cm^{-1}$ according to Okuyama and Satake (*31*). For calculation of the concentration of TNP-modified S1 (TNP-S1) the absorbance at 280 nm was corrected according to the formula: $\text{corrected}(A_{280}) = \text{observed}(A_{280}) - 0.362 \times \text{observed}(A_{345})$. Labeling specificity was also investigated with Mg^{2+}, Ca^{2+}, and K^+-EDTA ATPase measurements. S1 modified by TNBS under these circumstances had a (mole of TNP)/(mole of S1) ratio of 1 with 70−80% of the attached probe at RLR.

The reactive thiol in S1 was modified with IAF according to published protocols (*32*). S1 (10−25 μM) was modified with a 1.2-fold molar excess of IAF for 12 h at 4 °C in 0.2 mM PMSF and 25 mM TES, pH 7.0. Excess dye was removed by gel filtration on a PD10 column into S1 buffer (see below) and then exhaustive dialysis. This procedure produced fluorescein-labeled S1 (F-S1) with 60−70% of the SH1's modified and no detectable nonspecific label (*32*).

Solutions and Mixing Procedure for S1 and Actin + S1 Experiments. Experiments on S1 without actin were conducted in S1 buffer consisting of 0.1 mM PMSF, 60 mM KCl, and 25 mM HEPES, pH 8.

G-actin was stored in a buffer consisting of 0.2 mM $CaCl_2$, 0.2 mM DTT, 0.1 mM PMSF, 0.2 mM ATP, 0.005% sodium

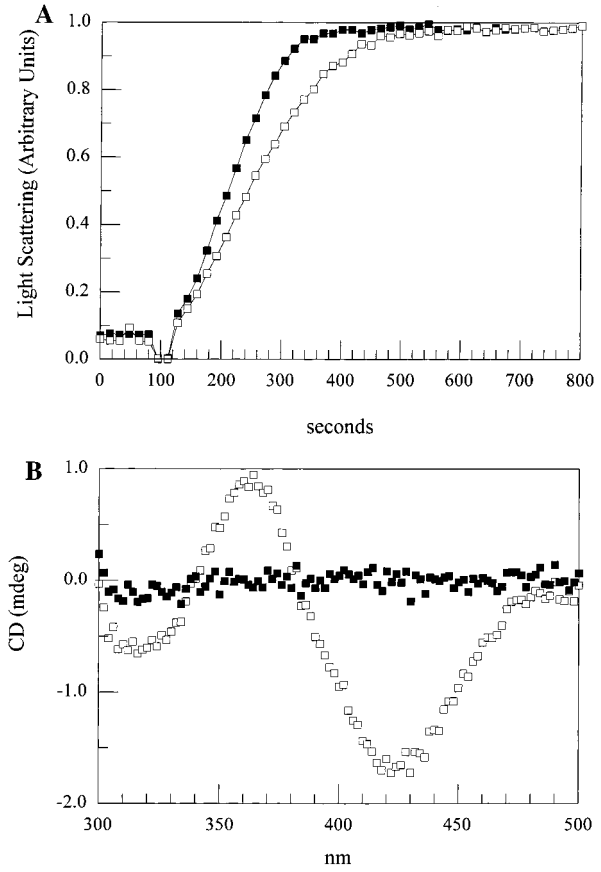

FIGURE 2: (A) Time course of 600 nm light scattering from a 2:1 mixture of actoS1 (■) and actoTNP-S1 (□). The G-actin concentration is 8 μM. Experiments were conducted in a 1 cm fluorescence cuvette with a sample optical density of ≤0.1. (B) CD spectra from actoS1 (■) and actoTNP-S1 (□) 10 min after the mixing of G-actin with S1 or TNP-S1 in a 2 cm path length cell. No detectable optical artifact is observed in the control actoS1, implying that spectra from actoTNP-S1 are quantitative.

azide, and 5 mM HEPES, pH 8. To remove free ATP from the actin before the actoS1 experiment, a gel filtration step was performed on a PD10 column in 0.2 mM $CaCl_2$, 0.2 mM DTT, 0.1 mM PMSF, and 5 mM HEPES, pH 8. Once exchanged, the G-actin was stored on ice and tested for functionality before each experiment by measuring its ability to polymerize.

We polymerized actin by adding S1 to the G-actin solution in the absence of MgATP using a procedure similar to that of Miller at al. (*33*). The properties of this polymerized actin are nearly identical to that polymerized by salt in the presence of MgATP. We used a 2:1 actin:S1 ratio at an actin concentration of 8 μM. The low protein concentrations slowed actin polymerization and limited polymer length, eliminating birefringence and scattering artifacts from our spectroscopic measurements. Complex formation was followed by measuring the time dependence of the light scattering at 600 nm.

Figure 2A shows 600 nm light scattering as a function of time from an actin + S1 or actin + TNP-S1 mixture. ActoS1 polymerized with a characteristic half-time $\tau_{1/2}$ ~100 s and reached steady state in ~5 min. The actin + TNP-S1 mixture polymerized more slowly ($\tau_{1/2}$ ~200 s) reaching steady state in ~7 min. Similar time constants were obtained for mixtures of actin + F-S1. Subsequently, we refer to this polymerized actin as filamentous or F-actin. Figure 2B shows CD spectra from actoS1 (■) or actoTNP-S1 (□) in a 2 cm path length cell collected with identical CD measuring conditions. Collection of the CD spectra was initiated 10 min after the mixing of G-actin with S1 or with TNP-S1 and finished within 2 min. Figure 2B shows we can quantitate the CD signal originating from the TNP in S1 (or from IAF in S1 because the F-S1 signal has larger contrast from the background actoS1 signal), which is structurally interpretable in terms of the probe/protein conformation, without significant contribution from any artifact optical activity due to the presence of the actin polymer.

Table 1: Fractional Percentage of Uncomplexed S1 in ActoS1 Samples[a]

	MgADP (μM)				
	0	25	200	500	1000
S1 + actin	3	n.o.	2.0	7.53	7.83
TNP-S1 + actin	3.3	n.o.	3.6	11.9	14.2
F-S1 + actin	9	3	n.o.	n.o.	n.o.

[a] n.o. is not observed.

The effect of MgADP binding to S1 in the presence of actin was studied by adding MgADP to polymerized actoS1 in the steady state. We added MgADP to actoS1 or actoTNP-S1 5 or 7 min after mixing G-actin with the S1. The addition of MgADP to the polymer decreased light scattering 5−10%, establishing a new steady-state intensity level within ~3 min such that the combined system was in steady state ~10 min after mixing G-actin and S1. For experiments with actin + S1 or F-S1 in the presence of MgADP, $MgCl_2$ and ADP were added to obtain final concentrations of 1 mM $MgCl_2$ and 25 μM ADP. This ADP concentration was sufficient to saturate the actin-bound S1 or F-S1 (*34*). For experiments with actin + TNP-S1 in the presence of MgADP, $MgCl_2$ and ADP were added to obtain final concentrations of 0.2−1.0 mM $MgCl_2$ and ADP. In this nucleotide concentration range, 30−80% of the actin-bound TNP-S1 active sites are occupied (A. Muhlrad, private communication).

Stoichiometry of the ActoS1 Complex. Native and modified S1's were mixed with G-actin under the conditions for formation of the actoS1 complex. After 10 min incubation the mixture was centrifuged at 200000*g* for 50 min; then the supernatant and pellet were separated. Material from each species was run on a 15% SDS−PAGE gel. The pellets contained a stoichiometric (1:1) complex of actin and S1, and nonpolymerized actin remained in the supernatant. Densitometric scans of the Coomassie-stained gels from the supernatant quantified the amount of uncomplexed S1 in the actoS1 mixture. These results, summarized in Table 1, show that 85−97% of the S1 and the labeled S1 were in complex with the F-actin during our spectroscopic measurements.

Formation of Trapped Complexes. S1, F-S1, or TNP-S1 (17−30 μM) was incubated in 60 mM KCl, 1 mM $MgCl_2$, 5 mM KF, 0.2 mM ADP, and 30 mM HEPES, pH 7.0 at 25 °C, for 5 min. Then 0.2 mM $BeCl_2$ or 0.2 mM $AlCl_3$ (0.6 mM for F−S1) was added and the incubation continued at 25 °C for 20 min. Stable trapped complex formation was followed by measuring the loss of Ca^{2+}-ATPase activity (*35*). In these conditions ≥90% of the active sites of the S1's are trapped.

Light Scattering. ActoS1 scattering of 600 nm wavelength light was observed at 90° from the excitation beam propaga-

Scheme 1

$$\begin{array}{ccccccccc} M + ATP & \leftrightarrow & M^{*}\bullet ATP & \leftrightarrow & M^{**}\bullet ADP\bullet Pi & \leftrightarrow & M^{\wedge}\bullet ADP + Pi & \leftrightarrow & M + ADP \\ \updownarrow & & \updownarrow & & \updownarrow & & \updownarrow & & \updownarrow \\ A\bullet M + ATP & \leftrightarrow & A\bullet M^{*}\bullet ATP & \leftrightarrow & A\bullet M^{**}\bullet ADP\bullet Pi & \leftrightarrow & A\bullet M^{\wedge}\bullet ADP + Pi & \leftrightarrow & A\bullet M + ADP \end{array}$$

tion direction. Measurements were made using a 1 cm path length cuvette on samples with optical density of ≤0.1 at 20 °C. Experiments were conducted on a SLM 8000 spectrofluorometer (SLM instruments, Urbana, IL).

Absorption and Circular Dichroism. Absorption spectra were measured on a Beckman DU650 (Beckman Instruments, Fullerton, CA) or a Cary 4E (Varian, Mulgrave Victoria, Australia) spectrophotometer. CD spectra were recorded on a JASCO J715 spectropolarimeter (Tokyo, Japan). Protein CD spectra measurements were carried out in a thermostated cell at 20 °C containing ~20 μM F^- or TNP-S1 in S1 buffer or 4 μM F^- or TNP-S1 with 8 μM actin in actin buffer. In addition, the sample may have contained nucleotides and phosphate analogues as described in the various experiments. To obtain a spectrum, CD was recorded from a sample containing modified S1 and subtracted from this was a similarly recorded spectrum from an identical sample with native S1.

The absorption dipole, $\langle 0|\vec{\mu}|j\rangle$, or extinction coefficient, $\epsilon_j(\lambda)$, gives the calculated or observed electric transition dipole strength for the jth electronic transition, D_j, by (*36*)

$$D_j = |\langle 0|\vec{\mu}|j\rangle|^2 = 9.18 \times 10^{-3} \int \frac{n\epsilon_j(\lambda)}{\lambda\beta^2} d\lambda \quad (\text{Debye}^2) \quad (1)$$

where λ is wavelength, $\langle 0|$ and $|j\rangle$ are the ground and excited state molecular orbital wave functions, and $\beta = (n^2 + 2)/3$ for the protein imbedded in a medium of refractive index n. The transition magnetic dipole, $\langle j|\vec{m}|0\rangle$, or CD extinction coefficient, $\Delta\epsilon_j$, gives the calculated or observed rotary strength for the jth electronic transition, R_j, by (*36*)

$$R_j = \text{Im}[\langle 0|\vec{\mu}|j\rangle \cdot \langle j|\vec{m}|0\rangle] = 0.248 \int \frac{\Delta\epsilon_j(\lambda)}{\beta\lambda} d\lambda \quad (\text{D-B}) \quad (2)$$

where D-B is Debye-Bohr magnetons.

Calculation of the Optical Signal. CD and absorption signals from the probes, IAF and TNP, modifying SH1 and RLR, respectively, were computed as described previously (*15*, *25*). Fluorescence polarization ratios for IAF-modifying SH1 in muscle fibers were computed as described in part 1. All trial S1 structures were generated by swiveling at the three conserved glycines, 699, 703, and 710, with the initial guess taken from either the "open" no-nucleotide crystal structure of skeletal S1 (*5*) or the "closed" ADP−AlF_4^--trapped crystal structure of smooth muscle S1 (*6*).

Pivoting the backbone at selected residues modifies the crystallographic structure to simulate the conformation changes occurring during hydrolysis that affect the local probe/S1 interactions. Changing probe/protein interactions alter the local probe environment and its spectroscopic signature. Probe spectroscopic signals also sense experimental conditions, for instance, pH and temperature (experimental conditions affect S1 conformation as well). As described above, we used two experimental conditions: (i) the conditions for all experiments except those with actin and (ii) the actin conditions. Conditions (i) are closer to the physiological and allow easy comparison of data between purified S1 and cross-bridges assembled in the muscle fiber. They are also the conditions from our previous work. Actin conditions (ii) were necessary to introduce actin to our purified S1 samples. We neutralized the effect of experimental conditions on the calculated optical signal by using the appropriate model spectra.

Relating Muscle Fiber and Solution Conformations of S1. Scheme 1 summarizes the elementary steps in ATP hydrolysis and force production by S1, where M is myosin and A is actin (*37*−*39*). In Scheme 1, M*, M**, and M^ represent distinct conformational states of M assumed during the ATPase cycle. The M**·ADP·P_i ↔ M^·ADP + Pi step is rate limiting in myosin ATPase (*37*) and is thought to be the power stroke in the presence of actin. Nucleotide, nucleotide analogues, and/or actin binding to S1 in solution produce some of the S1 intermediates of the cycle statically allowing their structural characterization with time-averaged signals. Nucleotide analogues MgADPBeF_x or MgADPAlF_4^- trapping the active site of native or probe-modified S1 in solution statically mimic the M*·ATP or M**·ADP·P_i intermediates, respectively (*35*, *40*−*42*). MgATPγS, when bound to the active site of myosin, mimics the M*·ATP intermediate (*43*). Actin binding to probe-modified S1 in solution in the absence and presence of MgADP statically produces intermediates A·M and A·M^·ADP.

In muscle fibers, static cross-bridge states include A·M and A·M^·ADP, i.e., rigor and MgADP states. Relaxed cross-bridges (from fibers in the presence of MgATP but no Ca^{2+} to activate contraction) are in dynamic equilibrium between weakly actin attached and dissociated states (i.e., A·M*·ATP ⇄ M*·ATP) (*44*). At low ionic strength the equilibrium shifts toward the weakly actin attached state, providing a means to characterize A·M*·ATP. Isometrically contracting fibers contain predominantly cross-bridges in the steady-state intermediate A·M**·ADP·P_i.

Our objective, to observe structurally sensitive signals from as many of the intermediates in Scheme 1 as possible and then to assign a structure for each of them, requires (i) the introduction of actin to the studies of S1 conformation in solution and (ii) the integration of solution-derived data to data obtained from the cross-bridges in intact muscle fibers. The most favorable experimental conditions for investigating the structure of a given state of the cross-bridge are when both solution and fiber studies are possible because we can do different experiments on each system. On muscle fibers we observe fluorescence polarization signals from 5′-iodoactamidofluorescein (IAF) modifying SH1 as described in part 1. On proteins in solution we observe CD and absorption signals from IAF-modifying SH1 in S1 or TNBS-modifying RLR. Only the data from IAF is integrable between fiber and solution studies of S1 conformation.

Table 2: Experimentally Characterized Cross-Bridge States from Scheme 1[a]

state (Scheme 1)	model system	comment
M	TNP-S1 and F-S1 in solution	
M*·ATP	$MgADPBeF_x$-trapped or MgATPγS-bound TNP-S1 and F-S1 in solution	pseudo-integrable with fiber A·M*·ATP
M**·ADP·P_i	$MgADPAlF_4^-$-trapped TNP-S1 and F-S1 in solution	pseudo-integrable with fiber A·M**·ADP·P_i
M^·ADP	MgADP-bound TNP-S1 and F-S1 in solution	
A·M	TNP-S1 and F-S1 with F-actin in solution	integrable
	IAF-labeled muscle fiber in rigor	
A·M*·ATP	IAF-labeled muscle fiber in low μ relax	pseudo-integrable with solution M*·ATP
A·M**·ADP·P_i	IAF-labeled muscle fiber in isometric contraction	pseudo-integrable with solution M**·ADP·P_i
A·M^·ADP	MgADP-bound TNP-S1 and F-S1 with F-actin in solution	integrable
	IAF-labeled muscle fiber with bound MgADP	

[a] CD and absorption are observed from labeled proteins in solution. Fluorescence polarization is observed from labeled muscle fibers.

Table 2 lists cross-bridge states for which structure constraining measurement were made. States with integrable observations from fibers and proteins in solution are noted. There are no static solution S1 states equivalent to A·M*·ATP and A·M**·ADP·P_i. They are the weak binding and the prepower stroke states inducible in a fiber with low ionic strength relaxed and isometric contraction conditions. The low ionic strength relaxed cross-bridge was already closely identified with the M*·ATP intermediate (*44*). Furthermore, it has been surmised from the crystallographic structures of S1 that a large lever arm rotation occurs with the M**·ADP·P*i* → M^·ADP transition (*6*). Associating this conformation change with the work producing lever arm rotation, we identify M**·ADP·P_i with the isometrically active cross-bridge. For these reasons, observations from A·M*·ATP and A·M**·ADP·P_i are noted in Table 2 as pseudo-integrable with M*·ATP and M**·ADP·P_i.

RESULTS

Absorption and CD Spectroscopy from F-S1 and TNP-S1. Figure 3A shows CD spectra from fluorescein in F-S1 in the absence and presence of nucleotide or nucleotide analogues at pH 7. These spectra represent the M (■), M*·ATP (□), M**·ADP·P_i (●), and M^·ADP (○) myosin intermediates without actin (see Scheme 1). Figure 3B shows CD spectra from F-S1 and F-S1 + MgADP in the absence and presence of actin at pH 8. These spectra represent the M (■), A·M (□), M^·ADP (○), and A·M^·ADP (●) myosin intermediates. There is large contrast among these signals, and in particular, the addition of F-actin has large but opposite effect on the F-S1 spectrum depending on whether MgADP is present. These data clearly demonstrate that, like MgADP and the nucleotide analogues, the binding of F-actin to F-S1 has a significant effect on the conformation of interface I. Table 3 contains a quantitative summary of all of the absorption and CD data from F-S1.

Figure 4 shows CD spectra from TNP-S1 under conditions identical to those in Figure 3. The contrast among these signals without actin (Figure 4A) clearly demonstrates that MgADP and the nucleotide analogues have a significant effect on the conformation of interface II. This result parallels that for fluorescein in interface I. The effect of the addition of actin on the TNP signal (Figure 4B) has consequences unlike those observed in interface I. We find that MgADP release from the A·M^·ADP complex, a step in the cross-bridge cycle of a muscle fiber, perturbs the TNP signal very little, suggesting interface II conformation is minimally changed. The spectra in Figure 4B further suggest that actin

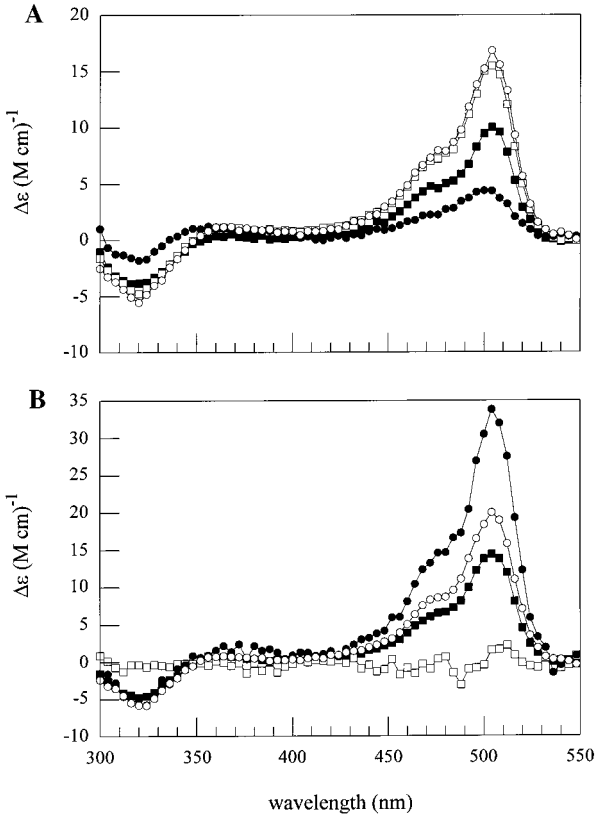

FIGURE 3: F-S1 CD spectra from ATPase states in the contraction cycle. (A) CD in the absence of actin at pH 7 from F-S1 (■), $MgADPBeF_x$-F-S1 (□), $MgADPAlF_4^-$-F-S1 (●), and MgADP-bound F-S1 (○). (B) CD in the presence and absence of actin at pH 8 from F-S1 (■), MgADP-bound F-S1 (○), F-actin + F-S1 (□), and F-actin + F-S1 + MgADP (●).

binding reverses the conformation change in interface II induced by the binding of MgADP to TNP-S1. Table 4 contains a quantitative summary of all of the absorption and CD data from TNP-S1.

Data in Figures 3 and 4 (summarized in Tables 3 and 4) identify conformational features common to interfaces I and II in the absence of actin that are reflected in the probe CD signals. First, rotary strengths from all observed probe absorption bands are similar for $MgADPBeF_x$-trapped and MgADP-bound probe-modified S1. Second, rotary strength amplitude from all observed probe absorption bands undergoes a dramatic reduction upon $MgADPAlF_4^-$ trapping of the active site of probe-modified S1. The first observation points out a known similarity between M* and M^ structural intermediates. The second shows that the interfaces remarkably produce a common response in the probes upon

Table 3: Quantitative Summary of Observed (Calculated) CD and Absorption Spectral Properties of F-S1[a]

	pH 7				
	5′IAF	F-S1	F-S1 + MgADP	F-S1 + MgADPBeF$_x$	F-S1 + MgADPAlF$_4^-$
λ_1 (nm)	492.7	500.2 (494)	501.0 (501)	501.0 (501)	497.8
λ_2	317.0	318.1 (317)	318.9 (317)	318.9 (317)	318.9
D_1 (D^2)	41.9	41.6 (42.3)	41.0 (40.5)	41.4 (42.3)	39.3
D_2	1.7	3.7 (1.4)	3.6 (1.4)	3.8 (1.4)	3.6
R_1 (D-B)	0	+0.168 (+0.168)	+0.283 (+0.284)	+0.261 (+0.261)	0.081
R_2	0	−0.098 (−0.023)	−0.123 (−0.102)	−0.113 (−0.102)	−0.04

	pH 8				
	5′IAF	F-S1	F-S1 + MgADP	F-S1 + F-actin	F-S1 + MgADP + F-actin
λ_1 (nm)	492.5	500.5	501.0	500.0 (494)	503.2 (503)
λ_2	317.0	320.4	320.9	320.7 (317)	321.5 (317)
D_1 (D^2)	44.1	48.1	49.1	33.6 (41.8)	36.8 (39.4)
D_2	3.2	2.4	2.3	5.5 (1.3)	8.0 (1.5)
R_1 (D-B)	0	+0.249	+0.341	0 (−0.011)	+0.590 (+0.569)
R_2	0	−0.102	−0.129	0 (+0.007)	−0.161 (−0.177)

[a] λ_i, D_i, and R_i are the peak wavelength for extinction, dipole strength, and rotary strength of the ith transition in nanometers (nm), Debyes (D), and Debye-Bohr magnetons (D-B), respectively. Excluding λ_i, measurement uncertainties are ∼10% principally due to error in the estimate of probe concentration. The estimates of peak wavelengths for extinction are ∼0.5 nm.

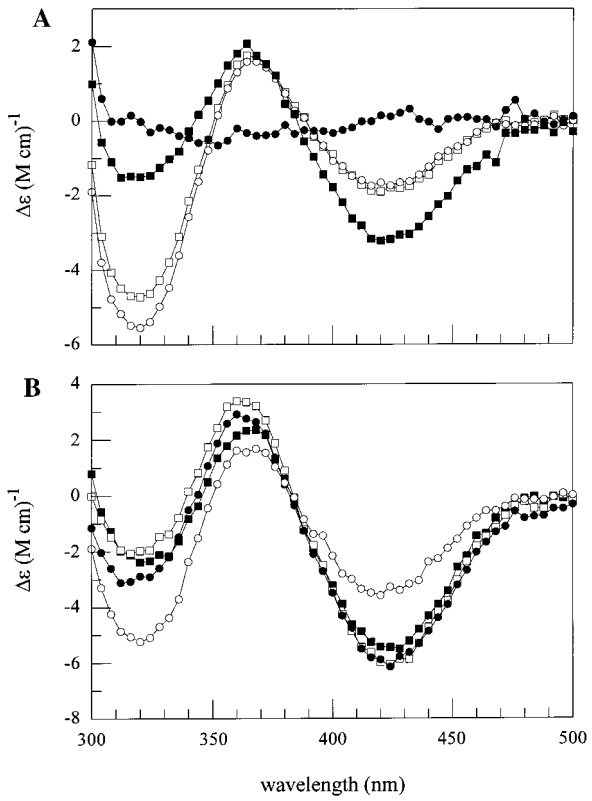

FIGURE 4: Same as in Figure 3 except with TNP-S1 substituted for F-S1. All MgADP-bound TNP-S1 spectra contained 0.5 mM MgADP.

formation of the M** structural intermediate. Possibly M** formation causes the loosening of local probe/protein contacts, permitting substantial independent probe movement and static averaging of a highly variable probe CD signal. This scenario is compelling for the TNP probe as we will see subsequently that TNP/protein contacts are minimized in M**. The situation for fluorescein and interface I in M** that we will see is less transparent although probe loosening remains a reasonable possibility.

Conformation of the Myosin Cross-Bridge. The best choices for the local and global probe/protein conformations were decided by minimizing the difference between the computed signals and experimental data. Adjustable parameters were dihedral angles conforming the modified side chain and probe to its binding site, each probe had an independent set of these parameters, and the Ramachandran angles for the conserved glycines 699, 703, and 710. The Ramachandran angles were identical for probes under equivalent physiological conditions. Experimental observations from the fluorescein probe in interface I consisted of fluorescence polarization from muscle fibers (part 1) and, CD and absorption data from F-S1 in solution in the presence and absence of F-actin. Experimental observations from the TNP probe in interface II consisted of CD and absorption data from TNP-S1 in solution in the presence and absence of F-actin. The one exception was isometrically active cross-bridges modeled using smooth muscle myosin coordinates. For this case we compared observed and computed fluorescence polarization signals from IAF at SH1 but did not attempt to fit the other spectroscopic data all taken from rabbit myosin S1. Figures 5−8 summarize selected best choices for S1 conformations.

Conformation of Interface I during Contraction. Figure 5 shows the polymer backbone, Trp510, and IAF-modifying SH1 of myosin at interface I in states representing those present in a contracting muscle fiber. The actin polymer axis, vertical and parallel to the long coordinate axis in the middle of the figure, is common for the left and right panels. The backbone atoms shown are within ∼15 Å of Trp510. The bolded backbone atoms correspond to His755−Ala769 from the converter domain contribution to the interface (except for the MgADP state where bolded atoms correspond to Phe760−Val765 to avoid overlap with those from rigor). The view is from the interior of S1 looking down the helix formed by residues 475−509 (the switch-2 helix) toward Trp510. The left panel shows interface I from an isometrically active cross-bridge as modeled by smooth muscle myosin (see Table 2). The right panel shows the superposition of skeletal myosin atoms in the presence of MgADP and in rigor. The isometrically active cross-bridge is displaced from the other structures for clarity. Lever arm movement during contraction, when the cross-bridge assumes the isometrically active,

Table 4: Quantitative Summary of Observed (Calculated) CD and Absorption Spectral Properties of TNP-S1[a]

	pH 7				
	TNP-Lys	TNP-S1	TNP-S1 + MgADP	TNP-S1 + MgADPBeF$_x$	TNP-S1 + MgADPAlF$_4^-$
λ_1 (nm)	417.1	422.0 (418)	418.5 (418)	419.0 (418)	422.2
λ_2	353.3	361.5 (354)	356.0 (354)	351.5 (353)	353.9
λ_3	330.8	329.2 (331)	329.0 (331)	329.0 (331)	333.5
D_1 (D^2)	9.7	8.5 (8.4)	7.9 (8.3)	7.8 (8.4)	9.5
D_2	12.9	4.4 (12.6)	5.1 (12.9)	7.0 (12.6)	10.5
D_3	5.1	18.2 (5.6)	18.3 (5.2)	14.9 (5.4)	26.3
R_1 (D-B)	−0.004	−0.099 (−0.099)	−0.050 (−0.061)	−0.052 (−0.054)	$\|R_1\| \leq 0.001$
R_2	−0.0002	+0.084 (+0.068)	+0.172 (+0.064)	+0.192 (+0.031)	$\|R_2\| \leq 0.01$
R_3	−0.002	−0.089 (−0.027)	−0.323 (−0.022)	−0.336 (−0.020)	$\|R_3\| \leq 0.01$

	pH 8				
	TNP-Lys	TNP-S1	TNP-S1 + MgADP	TNP-S1 + F-actin	TNP-S1 + MgADP + F-actin
λ_1 (nm)	415.1	421.3	420.8	422.7 (420)	422.1 (417)
λ_2	350.1	358.7	355.3	369.6 (354)	358.5 (354)
λ_3	320.6	338.8	337.0	329.8 (330)	329.1 (331)
D_1 (D^2)	10.2	9.8	9.1	8.9 (8.7)	8.8 (9.5)
D_2	11.6	4.6	4.2	9.0 (13.5)	8.5 (12.7)
D_3	5.1	12.3	10.1	13.8 (4.2)	13.9 (4.6)
R_1 (D-B)	−0.009	−0.170	−0.095	−0.167 (−0.155)	−0.179 (−0.159)
R_2	+0.008	+0.124	+0.159	+0.116 (+0.092)	+0.112 (+0.081)
R_3	−0.001	−0.132	−0.184	−0.083 (−0.023)	−0.120 (−0.036)

[a] The meaning of symbols and errors are as stated in the Table 3 footnote.

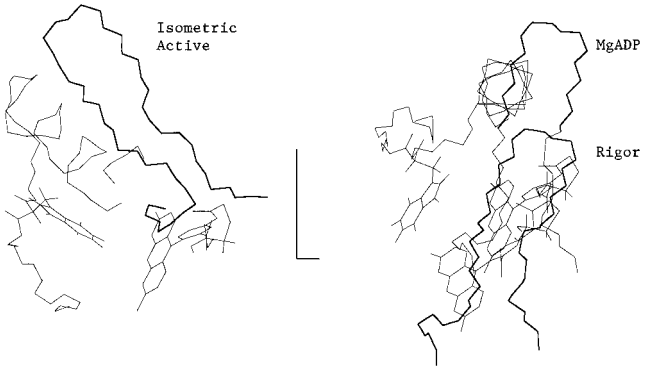

FIGURE 5: Interface I of myosin S1 during force generation. The left panel shows a smooth muscle myosin isometrically active cross-bridge. The right panel shows the superposition of skeletal myosin cross-bridges in the presence of MgADP and in rigor.

MgADP, and rigor conformation in a fiber, is visualized as the left to right tilting and translation of the bolded atoms from the lever arm. The switch-2 helix also translates and rotates in this representation.

Figure 6 shows a stereoview of the SH1 α-helix and IAF-modifying SH1 in rigor fibers. The peptide backbone wraps around the probe, and the xanthene is in close proximity to the conserved glycine swivel 710. The xanthene−glycine proximity may interfere with the swivel and possibly disrupts hydrogen bonding in the helix around Gly710. The carbonyl oxygen from Gly703 is 3.5 Å from the SH proton of Cys707 and the closest nonbonded atom in the crystal structure of skeletal S1 (*5*). Weak hydrogen bonding between these groups could lower the p*K* of this SH, explaining the anomalously high reactivity of Cys707 (*45*). Gly703 serves as a swivel during energy transduction, possibly further affecting the p*K* of Cys707 such that reactivity of SH1 depends on the conformation of the helix. This scenario is consistent with the observation that SH1 reactivity depends on the nucleotide bound to the active site of S1 (*46*).

Conformation of Interface II during Force Development in Contraction. Figure 7 shows the polymer backbone, Arg723, Glu776−777, Tyr85, and TNP-modifying myosin RLR at interface II in states representing those present during force development in a contracting muscle fiber. The view is from the interior of S1 looking down the α-helix of the lever arm. The backbone atoms shown are within ∼10 Å of RLR in the MgADP and rigor states. In the isometrically active state (bolded lines) RLR is more than 17 Å from the nearest backbone atom of the lever arm. Note that in this figure we have aligned the lever arms from the three states and allowed the catalytic domains to move. In this representation TNP-Lys84 and Tyr85 move from left to right for isometrically active, MgADP, and rigor states.

Independent movement of TNP at RLR is likely restricted by its interaction with Tyr85 and, in the case of the rigor cross-bridge, by interaction with Arg723, as reported previously in the absence of actin (*15*). Lever arm movement upon the binding of MgADP removes Arg723 from the vicinity of TNP. The lever arm movement when MgADP binds to actoS1 has larger amplitude than that in S1 alone where we observed the survival of the TNP-Arg723 interaction even in the presence of MgADP (*15*). Figure 7 shows that the negatively charged lever arm residue Glu776 replaces Arg723 as the side chain closest to the TNP in the MgADP state of the fiber. Glu776 was suggested to form a salt bridge with the unmodified Lys84 in the M* state of S1 on the basis of the crystal structure of *Dictyostelium* S1 (*47*). Since the M* and M^ states are structurally similar, as evidenced from the CD spectra from TNP-S1 in these states (Figure 4A), the proximity of TNP and Glu776 in the presence of MgADP is not surprising. Although both TNP and the side chain of Glu776 have negatively charged oxygen atoms, there is the possibility of a dipole−dipole attraction between them.

The conformation of the TNP probe at RLR in the isometrically active state, shown in Figure 7, was surmised by a local energy minimization calculation because we have no data for TNP-modifying RLR in smooth muscle; however,

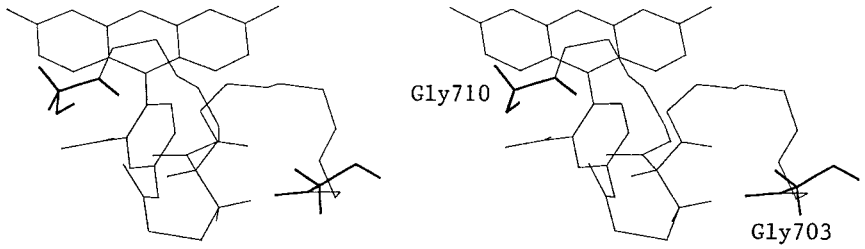

FIGURE 6: Stereoview of the α-helix containing SH1 and IAF modifying SH1 in rigor fibers.

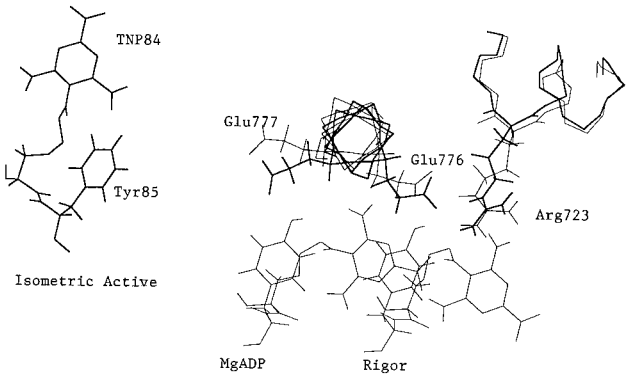

FIGURE 7: Interface II of myosin S1 showing the polymer backbone, Arg723, Glu776−777, Tyr85, and TNP modifying RLR in the isometrically active, MgADP, and rigor states of a muscle fiber. The backbone atoms shown are within ∼10 Å of RLR in the MgADP and rigor states. In the isometrically active state (bolded) RLR is more than 17 Å from the nearest backbone atom of the lever arm. The view is from the interior of S1 looking down the α-helix of the lever arm. Note that the lever arm is static but the catalytic domain moves in this representation of force development during contraction.

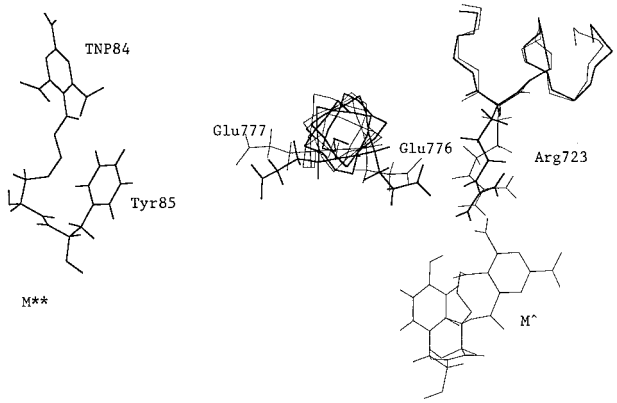

FIGURE 8: Interface II of myosin S1 showing the same atoms as in Figure 7 for the M**·ADP·P_i → M^·ADP transition during ATP hydrolysis without actin. Bolded atoms represent the M**·ADP·P_i state.

the accurate position of TNP is irrelevant to the following results. The distance between RLR and Glu776 is over 25 Å in the isometrically active state. RLR apparently loses contact with the lever arm in this conformation, unlike our previous suggestion based on a swiveling glycine model for M** in the absence of actin (*15*). The trajectory of RLR, intermediate to the three states depicted in Figure 7, is unknown. The path carrying the isometrically active to the MgADP states, the power stroke, probably brings RLR near to the lever arm, stopping within a salt bridge length of Glu776. If RLR carries the bulky TNP group, it collides with the lever arm.

Figure 8 shows lever arm motion for the M**·ADP·P_i → M^·ADP transition during ATP hydrolysis without actin. There the M**·ADP·P_i (bold) intermediate is taken directly from the MgADPAlF_4^- trapped smooth muscle S1 crystal structure (*6*), and the conformation of the TNP at RLR is identical to that in Figure 7. As shown, the M** conformation minimizes probe/protein contacts, possibly permitting substantial independent probe movement. Independent probe movement and the accompanying static averaging of a highly variable probe CD signal might explain why formation of the M**·ADP·P_i intermediate causes a substantial amplitude reduction in the probe CD signal (Figure 4A). The conformation change in the M**·ADP·P_i → M^·ADP transition is similar to the power stroke shown in Figure 7 and also shows the potential for a collision between TNP and the lever arm. This collision, if it occurs, could be responsible for the alteration of S1 ATPases when TNP modifies RLR, as suggested previously (*15*).

DISCUSSION

The structural characterization of S1 during contraction is the surest means to illuminating the energy transduction mechanism in myosin. Our spectroscopic approach is broadly applicable to the complicated intact muscle fiber system but less definitive than ideal when assigning the atomic structural basis for a spectroscopic signature. The structural assignment of the spectroscopic signature of S1 is a challenging problem because the information available from the observables does not uniquely specify the structure of the signal source. We reduce the complexity of the problem by restricting investigation to two interesting regions of the S1 by targeting them with two extrinsic probes. We reduce the intrinsic ambiguity in the observables by integrating contributions from multiple probe signals generated with different spectroscopic techniques. Specifically, we have identified interfaces I and II where the catalytic, converter, and lever arm domains interface (Figure 1) as our foci of interest and have integrated CD, absorption, and fluorescence polarization signals from the probes of these regions.

Energy Transduction in Myosin. Energy transduction is the sum of structural changes in S1 that accompany ATP hydrolysis and force production. We model the process, summarized in Scheme 1, by progressive structural changes in the S1 that first hydrolyze ATP and then bind actin and produce force while releasing products. In part 1 we looked principally at lever arm movement as this is the most striking (global) structural feature of energy transduction in the cross-bridge. Here we focus on the structural changes in S1 local to the probe binding sites. These investigations are initiated to provide insight to the underlying mechanism of the energy transduction process.

The results are summarized in Figures 5−8 where we show the conformation of the two interfaces identified in Figure 1. Figures 5 and 7 show interface I and II conformations for a simple representation of cross-bridge force generation consisting of three actin-bound states observed from muscle fibers in isometric contraction, in the presence of MgADP, and in rigor, going from highest to lowest free energy. The starting structure for the isometrically active cross-bridge is the "closed" conformation of S1 (*48*) given by the $MgADPAlF_4^-$-trapped smooth muscle S1 crystal structure (*6*). The starting structure for the MgADP and rigor cross-bridge is the "open" conformation of S1 given by the skeletal S1 crystal structure (*5*). Both starting crystal structures were perturbed by swiveling at the three conserved glycines, 699, 703, and 710, to accommodate the structural changes caused by actin and/or nucleotide binding. This model of energy transduction addresses structural changes that well characterize the observed spectroscopic signature of the cross-bridge state but not the underlying mechanism in the process. The proposed transient S1 structures will be refined in the future from new crystal structures and with the use of better (functional) models for energy transduction.

Interface I. Insight into how to improve the energy transduction model is found in Figure 5 where interface I from closed and open forms of S1 is compared. We see that the switch-2 helix undergoes realignment in the transition from isometrically active to MgADP states. This movement was already described by Holmes and Geeves from comparison of smooth and skeletal muscle S1 crystal structures as the breaking of the helix at Val497 and rotation of the loop connecting the helix with Trp510 (*49*). Our alignment of the actin-bound structures gives similar implications and identifies these residues as playing a role in future elaborated models of energy transduction.

Trp510 is the ATP-sensitive tryptophan in skeletal myosin (*8*−*14*). The closed conformation of Figure 5 has the indole of Trp510 tucked between the switch-2 helix and the peptide backbone for this residue. The indole and fluorescein xanthene form nearly a 90° angle between their planes. In the open conformation the indole moves away from the switch-2 helix and forms a stacked complex with the xanthene. The closed conformation of Trp510 is more protected from solution, explaining its reduced accessibility to collisional quenching when compared to the open form (*8*). Collisional quenching of Trp510 also distinguishes among the open forms of S1 with and without nucleotide in the absence of actin, although the contrast between them is less than between the open and closed conformations. These smaller differences in quencher accessibility might be due more to the converter or lever arm domain movement, like that seen in Figure 5 for the MgADP and rigor states, than to movement of the indole.

The SH of cysteine in solution has a p*K* of ∼8.5, but SH1 or Cys707 in S1 is highly reactive at neutral pH. The likely cause of the anomalous p*K* is a presence of a proton acceptor. The nearest candidate proton acceptor is the carbonyl oxygen of Gly703, a residue that acts as a swivel in the energy transduction mechanism of S1. As such, the proximity of the carbonyl oxygen to the SH varies with the nucleotide bound to the active site of S1, possibly indirectly changing Cys707 reactivity as observed for skeletal myosin S1 (*46*). The converse, that modifying Cys707 affects energy transduction, is true as well since the S1 ATPases are known to detect this modification (*50*).

How Ca^{2+}, Mg^{2+}, and K^+-EDTA ATPases change upon SH1 modification are specific to the modifier. For instance, iodoacetamide modification of SH1 activates Ca^{2+}-ATPase ∼8-fold, IAF causes a 5-fold activation, and bimane causes a 2-fold inhibition (*51*). These observations suggest that altered ATPases are not caused by an interference with proton sharing between Gly703 and Cys707, since this would happen equally well for all modifiers, but are because of steric interference between the modifying group and swiveling at the nearby glycine, whether Gly703 or Gly710. Figure 6 shows IAF interacting with Gly710 possibly interfering with the swivel. Iodoacetamide, a much smaller molecule than IAF, cannot reach Gly710 but is appropriately sized to interfere with swiveling at Gly703. The characteristic ability of the modifiers of SH1 to alter ATPases perhaps depends on which glycine swivel it perturbs.

Interface II. Figure 7 shows interface II under conditions identical to those in Figure 5. The conformation of S1 during force development in contraction, viewed from the perspective of RLR, has this charged residue moving a large distance from an environment where it has no local interactions, except with neighboring residues of the catalytic domain in the isometric active state, to an encounter with the converter and/or lever arm domains in the MgADP and rigor states. The MgADP and rigor states are similar and offer RLR a more structured environment due to the proximity of the other domains. If RLR takes a trajectory between the isometrically active and MgADP states that allows clearance sufficient only to avoid clashes with the lever arm in native S1, then when TNP modifies RLR, the probe will directly collide with the lever arm.

We surmised a similar collision between the lever arm and TNP-modified RLR during ATP hydrolysis without actin (*15*). There the bulky TNP group was thought to interfere with the M*·ATP → M**·ADP·P_i transition (Figure 8), causing both the inhibition of K^+-EDTA ATPase and the acceleration of the Mg^{2+}-ATPase: the former by increasing the internal resistance to the M*·ATP → M**·ADP·P_i transition, thereby halting or subverting the monovalent cation ATPase, and the latter by destabilizing the predominant intermediate, M**·ADP·P_i, by preventing the normally stabilizing interactions between the catalytic domain near to RLR and the converter and/or lever arm domains. In the presence of actin, a collision between TNP and the lever arm would inhibit force generation or work production at the A·M**·ADP·P_i ↔ A·M^·ADP transition, i.e., the power stroke. If so, then TNP-S1 will be unable or less able to do work, and the path of lever arm movement during the A·M**·ADP·P_i ↔ A·M^·ADP transition will be better defined since it must move in a trajectory allowing the TNP/lever arm collision.

Conclusions. Open and closed S1 crystal structures were extrapolated to working "in solution" or oriented "in tissue" forms using a simplified working model of energy transduction. The model generates structure-sensitive optical spectroscopic signals for comparison with observed signals from extrinsic probes located at two different interfaces within S1 containing the catalytic, converter, and lever arm domains. Interface I contains SH1 and the ATP-sensitive tryptophan, Trp510. The conformation of interface I during

ATPase and force development in contraction suggests the molecular basis for Trp510 collisional quenching sensitivity to nucleotide binding. The conformation of the SH1-bound probe also suggests how it alters S1 ATPases. Interface II contains RLR. At interface II, the spatial relationship of the lever arm and the TNP at RLR suggests how the probe alters S1 ATPases and that it should inhibit lever arm movement during the power stroke. The latter possibility, if true, would establish a part of the corridor through which the lever arm swings during the power stroke.

ACKNOWLEDGMENT

We thank Dr. A. Muhlrad (Hebrew University, Jerusalem, Israel) for giving us access to data on the binding of MgADP to TNP-S1, Dr. György Hegyi (Eötvös Loránd University, Budapest, Hungary) for the muscle acetone powder used as the source of actin in all of our experiments, and Ms. S. P. Garamszegi for technical assistance on the project.

REFERENCES

1. Maita, T., Yajima, E., Nagata, S., Miyanishi, T., Nakayama, S., and Matsuda, G. (1991) *J. Biochem. 110*, 75−87.
2. Morales, M. F., and Botts, J. (1979) *Proc. Natl. Acad. Sci. U.S.A. 76*, 3857−3859.
3. Toyoshima, Y. Y., Kron, S. J., McNally, E. M., Niebling, K. R., Toyoshima, C., and Spudich, J. A. (1987) *Nature 328*, 536−539.
4. Kitamura, K., Tokunaga, M., Iwane, A. H., and Yanagida, T. (1999) *Nature 397*, 129−134.
5. Rayment, I., Rypniewski, W. R., Schmidt-Base, K., Smith, R., Tomchick, D. R., Benning, M. M., Winkelmann, D. A., Wesenberg, G., and Holden, H. M. (1993) *Science 261*, 50−58.
6. Dominguez, R., Freyzon, Y., Trybus, K. M., and Cohen, C. (1998) *Cell 94*, 559−571.
7. Houdusse, A., Kalabokis, V. N., Himmel, D., Szent-Gyorgyi, A. G., and Cohen, C. (1999) *Cell 97*, 459−470.
8. Park, S., Ajtai, K., and Burghardt, T. P. (1996) *Biochim. Biophys. Acta 1296*, 1−4.
9. Park, S., and Burghardt, T. P. (2000) *Biochemistry 39*, 11732−11741.
10. Papp, S., and Highsmith, S. (1993) *Biochim. Biophys. Acta 1202*, 169−172.
11. Hiratsuka, T. (1992) *J. Biol. Chem. 267*, 14949−14954.
12. Batra, R., and Manstein, D. J. (1999) *Biol. Chem. 380*, 1017−1023.
13. Bivin, D. B., Kubota, S., Pearlstein, R., and Morales, M. F. (1993) *Proc. Natl. Acad. Sci. U.S.A. 90*, 6791−6795.
14. Yengo, C. M., Chrin, L. R., Rovner, A. S., and Berger, C. L. (2000) *J. Biol. Chem. 275*, 25481−25487.
15. Ajtai, K., Peyser, Y. M., Park, S., Burghardt, T. P., and Muhlrad, A. (1999) *Biochemistry 38*, 6428−6440.
16. Kubo, A., Tokura, S., and Tonomura, Y. (1960) *J. Biol. Chem. 235*, 2835−2839.
17. Mornet, D., Pantel, P., Bertrand, R., Audemard, E., and Kassab, R. (1980) *FEBS Lett. 117*, 183−188.
18. Hozumi, T., and Muhlrad, A. (1981) *Biochemistry 20*, 2945−2950.
19. Muhlrad, A., and Takashi, R. (1981) *Biochemistry 20*, 6749−6754.
20. Fabian, F., and Muhlrad, A. (1968) *Biochim. Biophys. Acta 162*, 596−603.
21. Muhlrad, A. (1983) *Biochemistry 22*, 3653−3660.
22. Muhlrad, A. (1977) *Biochim. Biophys. Acta 493*, 154−166.
23. Burghardt, T. P., Cruz-Walker, A. R., Park, S., and Ajtai, K. (2001) *Biochemistry 40*, 4821−4833.
24. Edwards, R. A., and Woody, R. W. (1977) *Biochem. Biophys. Res. Commun. 79*, 470−476.
25. Burghardt, T. P., Garamszegi, S. P., Park, S., and Ajtai, K. (1998) *Biochemistry 37*, 8035−8047.
26. Tonomura, Y., Appel, P., and Morales, M. (1966) *Biochemistry 5*, 515−521.
27. Weeds, A. G., and Taylor, R. S. (1975) *Nature 257*, 54−56.
28. Pardee, J. D., and Spudich, J. A. (1982) *Methods Enzymol. 85*, 164−179.
29. Fiske, C. H., and Subbarow, Y. (1925) *J. Biol. Chem. 66*, 375−400.
30. Tashima, Y. (1975) *Anal. Biochem. 69*, 410−414.
31. Okuyama, T., and Satake, K. (1960) *J. Biochem. 47*, 454−462.
32. Ajtai, K., and Burghardt, T. P. (1992) *Biochemistry 31*, 4275−4288.
33. Miller, J., Phillips, M., and Reisler, E. (1988) *J. Biol. Chem. 263*, 1996−2002.
34. Aguirre, R., Gonsoulin, F., and Cheung, H. C. (1986) *Biochemistry 25*, 6827−6835.
35. Werber, M. M., Peyser, Y. M., and Muhlrad, A. (1992) *Biochemistry 31*, 7190−7197.
36. Schellman, J. A. (1975) *Chem. Rev. 75*, 323−331.
37. Bagshaw, C. R., and Trentham, D. R. (1974) *Biochem. J. 141*, 331−349.
38. Lymn, R. W., and Taylor, E. W. (1971) *Biochemistry 10*, 4617−4624.
39. Brenner, B. (1986) *Basic Res. Cardiol. 81*, 1−15.
40. Fisher, A. J., Smith, C. A., Thoden, J. B., Smith, R., Sutoh, K., Holden, H. M., and Rayment, I. (1995) *Biochemistry 34*, 8960−8972.
41. Peyser, Y. M., Ajtai, K., Werber, M. M., Burghardt, T. P., and Muhlrad, A. (1997) *Biochemistry 36*, 5170−5178.
42. Maruta, S., Henry, G. D., Sykes, B. D., and Ikebe, M. (1993) *J. Biol. Chem. 268*, 7093−7100.
43. Goody, R. S., and Hofmann, W. (1980) *J. Muscle Res. Cell Motil. 1*, 101−115.
44. Brenner, B., Schoenberg, M., Chalovich, J. M., Green, L. E., and Eisenberg, E. (1982) *Proc. Natl. Acad. Sci. U.S.A. 79*, 7288−7291.
45. Desiraju, G. R., and Steiner, T. (1999) in *The Weak Hydrogen Bond in Structural Chemistry and Biology*, pp 121−292, Oxford University Press, Oxford.
46. Phan, B. C., Peyser, Y. M., Reisler, E., and Muhlrad, A. (1997) *Eur. J. Biochem. 243*, 636−642.
47. Muhlrad, A., Peyser, Y. M., Ajtai, K., and Burghardt, T. P. (2001) Effect of ionic strength on the conformation of myosin subfragment 1−nucleotide complexes, *Biophys. J.* (submitted for publication).
48. Geeves, M. A., and Holmes, K. C. (1999) *Annu. Rev. Biochem. 68*, 687−728.
49. Holmes, K. C., and Geeves, M. A. (2000) *Philos. Trans. R. Soc. London, Ser. B 355*, 419−431.
50. Sekine, T., and Kielley, W. W. (1964) *Biochim. Biophys. Acta 81*, 336−345.
51. Ue, K. (1987) *Biochemistry 26*, 1889−1904.

BI002388G